JACS
JOURNAL OF THE AMERICAN CHEMICAL SOCIETY
Article
pubs.acs.org/JACS

Access to Cα Backbone Dynamics of Biological Solids by ^{13}C T_1 Relaxation and Molecular Dynamics Simulation

Sam Asami,[†] Justin R. Porter,[†] Oliver F. Lange,[†] and Bernd Reif*[,‡,†]

[†]Munich Center for Integrated Protein Science (CIPSM) at Department of Chemie, Technische Universität München (TUM), Lichtenbergstr. 4, D-85747 Garching, Germany

[‡]Helmholtz-Zentrum München, Deutsches Forschungszentrum für Gesundheit und Umwelt (HMGU), Ingolstädter Landstr. 1, D-85764 Neuherberg, Germany

Supporting Information

ABSTRACT: We introduce a labeling scheme for magic angle spinning (MAS) solid-state NMR that is based on deuteration in combination with dilution of the carbon spin system. The labeling strategy achieves spectral editing by simplification of the HαCα and aliphatic side chain spectral region. A reduction in both proton and carbon spin density in combination with fast spinning (≥50 kHz) is essential to retrieve artifact-free ^{13}C-R_1 relaxation data for aliphatic carbons. We obtain good agreement between the NMR experimental data and order parameters extracted from a molecular dynamics (MD) trajectory, which indicates that carbon based relaxation parameters can yield complementary information on protein backbone as well as side chain dynamics.

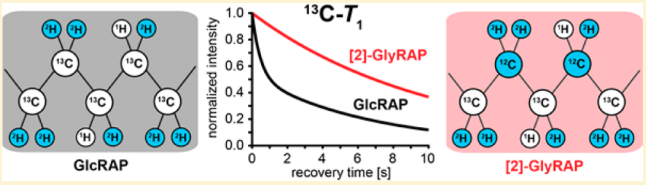

INTRODUCTION

In the past 10 years, solid-state NMR matured into a tool in structural biology that allows study of biological samples in crystalline, noncrystalline, and sedimented states.[1−6] NMR spectroscopy is particularly strong in the analysis of biomolecular dynamics. Understanding of dynamic processes is of fundamental interest, as motions on submillisecond time scales enable protein function despite the close packing in globular proteins.[7−9] In solution NMR, internal motions on a time scale greater than nanoseconds are difficult to detect, as they are masked by molecular tumbling. In the solid-state NMR, rotational diffusion is impaired. As a consequence, solid-state NMR is sensitive to internal motions on all time scales.

In the solid-state, coherent and noncoherent effects contribute to the experimental, apparent T_1 relaxation times. Coherent contributions are not easily removed and make an estimation of the dynamic contribution to the relaxation rates rather difficult.

Coherent effects are due to interactions among dipolar coupled spins. Spin diffusion, e.g., during the T_1 relaxation period, results in magnetization transfer, and yields an apparently shorter ^{13}C T_1 relaxation time of a certain nucleus, in case this spin is coupled to a relaxation "sink", which has a much shorter relaxation time.[10] Spin diffusion scales inversely with the magic-angle spinning (MAS) frequency.[11,12] Fast spinning at the magic angle can reduce the detrimental effects induced by spin diffusion.[13] In protonated samples, carbonyl ^{13}C T_1 relaxation times can potentially be quantified reliably. However, even at a MAS frequency of 60 kHz, spin diffusion results in a number of cross-peaks in particular in the aliphatic region of the ^{13}C,^{13}C PDSD spectra, indicating that spinning at this rotation frequency alone is not sufficient to suppress spin diffusion in protonated samples.[13] A further reduction in spin diffusion is required, which can potentially be achieved by proton spin dilution.[14,15,13]

On the other hand, obviously incoherent effects, such as ps-ns motions, contribute to T_1 relaxation times.[16−19] Quantification of internal dynamics is only possible, if these coherent and incoherent effects can be separated.

In this manuscript, we focus on the influence of spin diffusion and the separation of coherent and incoherent contributions to the experimentally determined ^{13}C T_1 relaxation times. We combine fast magic angle spinning and ^{1}H, as well as ^{13}C spin dilution. For that purpose, we suggest a labeling scheme, coined GlyRAP, which is an extension of the recently introduced reduced adjoining protonation (RAP) labeling scheme, yielding carbon spin dilution by an approach originally introduced by LeMaster and Kushlan.[24−28] The GlyRAP labeling simplifies spectra, increases the spectral resolution, enables spectral editing, and allows the artifact-free determination of ^{13}C relaxation rates. The experiments are demonstrated using a microcrystalline sample of the chicken α-spectrin SH3 domain. Proton detection experiments are employed to yield high sensitivity.

MATERIALS AND METHODS

Sample Preparation. GlcRAP samples of the SH3 domain of chicken α-spectrin were produced, as described earlier.[29,25] The protein expression was carried out with $^{15}NH_4Cl$, u-[^{2}H, ^{13}C] glucose

Received: September 11, 2014
Published: January 7, 2015

DOI: 10.1021/ja509367q
J. Am. Chem. Soc. 2015, 137, 1094−1100

and 15%/85%, 25%/75% H_2O/D_2O in the M9 minimal medium to produce the 15%, 25% GlcRAP sample, respectively. To produce the 10% [2]-GlyRAP sample, u-[^{2}H, 2-^{13}C] glycerol (Isotec, 2 g/L) instead of glucose was used. The medium was supplemented further with $Na^1H^{13}CO_3$ (2 g/L).[24] Prior to crystallization in 100% D_2O, all samples were lyophilized two times in D_2O at pH 3.5. 3.2 mm rotors were packed with microcrystals of a 25% GlcRAP sample using a tabletop centrifuge. 1.3 mm rotors were packed with microcrystals of a 15% GlcRAP and a 10% [2]-GlyRAP sample by ultracentrifugation (~20 min, 135000g) employing an ultracentrifuge device.[30] The rotors were sealed by gluing to increase the tightness of seal, as described previously.[27]

NMR Spectroscopy. NMR experiments were carried out using Bruker Biospin Avance spectrometers operating at ^{1}H Larmor frequencies of 500, 700, and 850 MHz, respectively, using commercial 3.2 and 1.3 mm triple-resonance probes. The 1.3 mm probe of the 850 MHz spectrometer was equipped with an additional external ^{2}H coil.[31] At all MAS frequencies, the effective sample temperature was adjusted to ~20−25 °C, using the chemical shift difference between the solvent resonance and L8δ2. At 700 MHz, the employed rf fields on the ^{1}H, ^{13}C and ^{15}N channels for hard pulses were 96, 61, and 50 kHz, respectively. At 500 MHz (850 MHz) rf fields of 167 (90−100), 100 (92−95) and 62.5 (100) kHz were applied on the ^{1}H, ^{13}C, ^{2}H (^{15}N) channel, respectively. Low-power ^{1}H, ^{2}H, ^{13}C decoupling of 2.5 kHz was applied, using the WALTZ-16 decoupling scheme.[32] $^{13}C\alpha$ backbone T_1 relaxation experiments were recorded using the pulse sequence depicted in Figure S5. In experiments carried out with the 25% GlcRAP sample, cross-polarization (CP) was employed for magnetization transfer and water saturation for solvent suppression (Figure S5A).[33,34] For the 10% [2]-GlyRAP and the 15% GlcRAP sample, a refocused INEPT scheme was employed (Figure S5B). During the recovery time 2nΔ, π pulses were applied after every time point Δ on the ^{1}H and ^{15}N channel to reduce cross-correlated relaxation.[35−37,22] $^{13}C\alpha$,^{15}N as well as $^{13}C\alpha$,^{2}H cross-correlation effects are marginal in comparison to $^{13}C\alpha$,^{1}H.[38] We note that $^{13}C\alpha$,^{1}H cross-correlation effects are small due to self-decoupling of two spin order terms containing ^{1}H, since the longitudinal relaxation time for protons is up to an order of magnitude shorter than for $^{13}C\alpha$.[39−41] To reduce systematic errors and the number of fitting parameters, the ^{13}C magnetization, prior to the T_1 recovery delay, was cycled as $+S_z$ and $-S_z$.[42] To obtain high sensitivity, both sequences were designed for ^{1}H detection.

Data Analysis. The spectra were processed in Topspin v2.1 and peak volumes extracted by box integration, using in-house Python scripts. The experimental error was set to two times the standard deviation of the noise and the uncertainty of the T_1 values was estimated by 1000 Monte Carlo runs.

^{13}C T_1 Relaxation in the Solid-State. Spin relaxation is particularly sensitive to ps-ns motions.[16−19] Nuclear relaxation is essentially induced by the modulation of the dipolar coupling between directly bonded proton and carbons due to motion. Additionally, modulation of the Chemical Shift Anisotropy (CSA) contributes to relaxation. The T_1 times are related to the ^{1}H,X (X = ^{13}C, ^{15}N) dipolar coupling anisotropy d, the CSA c, and the spectral density function $J_m(\omega)$ according to[43,20]

$$R_1 = \frac{1}{T_1} = \frac{1}{10}d^2[J_0(\omega_H - \omega_X) + 3J_1(\omega_X) + 6J_2(\omega_H + \omega_X)] + \frac{2}{15}c^2J_1(\omega_X)$$

with $d = \gamma_H\gamma_X\hbar/r_{HX}^3$ and $c = \gamma_C B_0 \Delta\sigma$. γ_H and γ_X are the gyromagnetic ratios for ^{1}H and X, respectively. $\hbar$ is the reduced Planck constant, and r_{HX} describes the ^{1}H,X distance. For backbone $^1H\alpha$,$^{13}C\alpha$ pairs, a value of 1.11 Å is employed.[44−46] The model-free formalism (MFF) links the motional amplitudes and correlation times to spin relaxation.[47−50] Clore et al. extended the method to account for two time scales of internal motions.[51] The spectral density within the extended MFF is given as

$$J_{solution}(\omega) = S^2\frac{\tau_r}{1+(\omega\tau_r)^2} + (1-S_f^2)\frac{\tau_f'}{1+(\omega\tau_f')^2} + S_f^2(1-S_s^2)\frac{\tau_s'}{1+(\omega\tau_s')^2}$$

with $1/\tau_f' = 1/\tau_f + 1/\tau_r$ and $1/\tau_s' = 1/\tau_s + 1/\tau_r$, while the generalized order parameter, S^2, can be written as the product of two order parameters, S^2_{fast} and S^2_{slow}, accounting for the amplitude of fast and slow motions, respectively. In solution, the first term describes the effect of molecular tumbling. In the solid-state, the spectral density function reduces to ($\tau_r \to \infty$)[52]

$$J_{solid}(\omega) = (1-S_f^2)\frac{\tau_f}{1+(\omega\tau_f)^2} + S_f^2(1-S_s^2)\frac{\tau_s}{1+(\omega\tau_s)^2}$$

The CSA is determined by the difference of the parallel and perpendicular components of the chemical shift tensor, $|\Delta\sigma| = |\sigma_{\parallel} - \sigma_{\perp}|$, and accounts for about 25−45% of ^{15}N ($\Delta\sigma$ = 170 ppm)[53,54] backbone T_1 relaxation, whereas insignificant CSA contributions less than 2% are expected for $^{13}C\alpha$ ($\Delta\sigma$ = 20 ppm)[55] at external magnetic fields of 14.1−23.5 T (Figure S4A). For the quantitative analysis of backbone T_1 relaxation data, in principle the CSA for all sites must be known since the CSA varies strongly along the primary sequence.[56−59] However, due to its small contribution to $^{13}C\alpha$ T_1, CSA can be safely neglected and elaborate experimental approaches can be omitted.

Analysis of ^{13}C Spin Diffusion. To simulate apparent ^{13}C T_1 relaxation times under the influence of ^{13}C,^{13}C spin diffusion, we assumed a simple model,[60,37,61,15]

$$L_A \overset{\rho_A}{\leftarrow} [A] \underset{\sigma}{\Leftrightarrow} [B] \overset{\rho_B}{\rightarrow} L_B$$

in which the carbon magnetization $[A]$ and $[B]$ of the spins A and B, respectively, decay with the autorelaxation rates ρ_A and ρ_B, while L_A and L_B describe the magnetization of the "lattice". To account for spin diffusion, the spin diffusion rate σ was introduced. The kinetic matrix can thus be written as

$$\frac{d}{dt}\begin{pmatrix}[A](t)\\ [B](t)\end{pmatrix} = -\begin{pmatrix}\rho_A + \sigma_{AB} & -\sigma_{AB}\\ -\sigma_{AB} & \rho_B + \sigma_{AB}\end{pmatrix}\begin{pmatrix}[A](t)\\ [B](t)\end{pmatrix} \quad (1)$$

The solution of the differential equation is given by

$$\begin{pmatrix}[A](t)\\ [B](t)\end{pmatrix} = \begin{pmatrix}\zeta(t)\{(1-e^{\lambda t})[A_0(\rho_A-\rho_B) - 2B_0\sigma] + (1+e^{\lambda t})A_0\lambda\}\\ \zeta(t)\{(1-e^{\lambda t})[-B_0(\rho_A-\rho_B) - 2A_0\sigma] + (1+e^{\lambda t})B_0\lambda\}\end{pmatrix} \quad (2)$$

with

$$\zeta(t) = \frac{1}{2\lambda}\exp\left[-\frac{1}{2}(\lambda + \rho_A + \rho_B + 2\sigma)t\right] \quad (3)$$

and

$$\lambda = \sqrt{4\sigma^2 + (\rho_A - \rho_B)^2} \quad (4)$$

MD Simulation. Molecular dynamics (MD) simulations were started from the crystal structure of the α-spectrin SH3 domain (PDB code: 2NUZ).[62] The 4 SH3 monomers of the asymmetric crystal unit were simulated in an orthorhombic crystal lattice using periodic boundary conditions with cell dimensions 34 × 43 × 50 Å. Simulations were carried out using the Amber99SB all-atom force field in GROMACS 4.5.4[63] with TIP3P water. The simulation system comprised 8 unit cells (2 × 2 × 2), containing 63437 atoms altogether, including 33705 solvent molecules, 114 Na^+ ions and 146 Cl^- ions. The salt concentration corresponds to 150 mM, the net

DOI: 10.1021/ja509367q
J. Am. Chem. Soc. 2015, 137, 1094−1100

charge is neutral. LINCS[64] and Settle[65] were applied to constrain covalent bond lengths, allowing an integration time step of 2 fs. Electrostatic interactions were calculated with the particle-mesh Ewald method.[66] The temperature was kept constant at 300 K by separately coupling (τ = 1 ps) the peptide and solvent to an external temperature bath using velocity-rescaling.[67] The pressure was kept constant employing Berendsen coupling (τ = 0.5 ps) to a pressure bath. The simulation was relaxed using steepest-descent followed by a 500 ps equilibration using position restraints on heavy atoms. After the equilibration phase, the simulation was within 0.2% of the experimentally observed unit cell volume. A MD simulation was run for 97 ns for an isothermal−isobaric ensemble (NPT). The correlation functions for Hα,Cα backbone vectors were calculated explicitly using this MD trajectory. Global molecular reorientations do not affect this calculation, as the molecule was restricted within the crystal lattice.[68−71] Subsequently, the parameters describing the extended model-free formalism[49,51] were fit using the formula

$$C(t) = S^2 + (1 - S^2_{\text{fast}})e^{-t/\tau_{\text{fast}}} + S^2_{\text{fast}}(1 - S^2_{\text{slow}})e^{-t/\tau_{\text{slow}}}$$

where S^2 corresponds to the generalized order parameter, $S^2 = S^2_{\text{fast}}S^2_{\text{slow}}$. τ_{fast} and τ_{slow} are the time scales of fast and slow internal motions, respectively.

RESULTS

GlyRAP Labeling and Spectral Editing. Reduced adjoining protonation (RAP) labeling enables the detection of aliphatic protons in the solid-state at already low MAS frequencies.[25−28] The protein is expressed, using uniformly deuterated and ^{13}C labeled glucose. These samples are referred to as GlcRAP samples in the following. Figure 1A shows a ^{1}H,^{13}C HMQC spectrum of a 25% GlcRAP sample of the SH3 domain of α-spectrin (using 25% H_2O/75% D_2O in the growth medium).

Overall, high resolution is achieved. However, resolution in the Cα region is compromised due to spectral crowding. Use of deuterated and 2-[^{13}C] labeled glycerol in the bacterial growth medium yields isotopic labeling at almost every second carbon (Figure S1).[24] The proton content of the protein can be tuned by adjusting the amount of H_2O/D_2O in the minimal medium. A sample for which 10% H_2O has been employed is termed 10% [2]-GlyRAP in the following. Figure 1B shows a ^{1}H,^{13}C HSQC spectrum for such a sample. Clearly, resolution is significantly improved as approximately only every second carbon is isotopically enriched. Because of the alternate labeling pattern, $^1J(^{13}C,^{13}C)$ couplings are removed yielding an additional enhancement in resolution. None, or very little incorporation of ^{13}C is expected for backbone Arg-Cα, Gln-Cα, Glu-Cα, Leu-Cα, Pro-Cα (Figure 1C,D) and about half of the side chain resonances (Figure 1E,F). For the methyls Ala-Cβ, Ile-Cγ2, Leu-Cδ1/-Cδ2, Met-Cε and Val-Cγ1/-Cγ2 resonances are suppressed (Figure 1G,H), enabling spectral editing.

^{13}C T_1 Relaxation Experiments. In the solid-state, molecular tumbling is absent and, therefore, relaxation is only determined by internal dynamics. By contrast, significant contributions to relaxation originate from molecular tumbling for proteins in solution. As a consequence, T_1 times vary only marginally in solution, whereas variations of roughly one order of magnitude can be found in the solid-state (Figure S4C). These results encouraged us to determine ^{13}C T_1 relaxation times in the solid-state.

In order to include ^{13}Cα T_1 data into an analysis of molecular dynamics in the solid-state, two major obstacles need to be overcome: On one hand, T_1 times in the solid-state are dependent on the crystallite orientation, and therefore magic angle spinning must be explicitly taken into account.[20] Powder averaging yields a multiexponentially decaying T_1 relaxation curve. It was shown that the initial slope is monoexponential which directly provides orientation-independent MAS powder

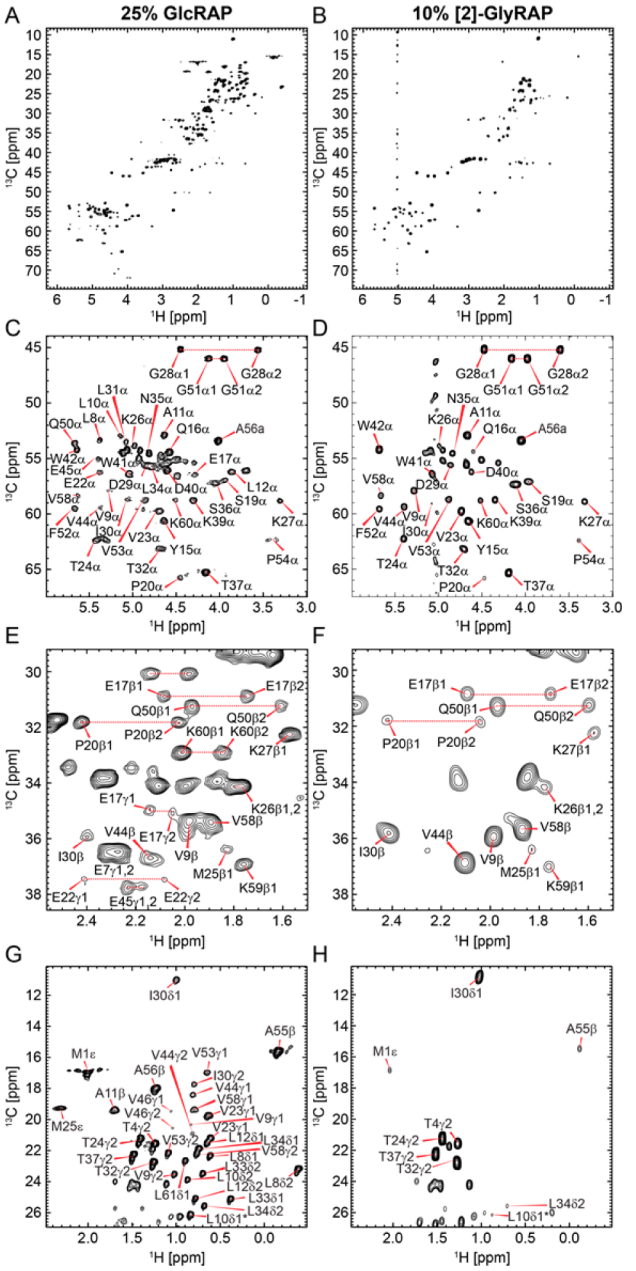

Figure 1. ^{1}H-detected ^{1}H,^{13}C correlation spectra of a (*left column*) 25% GlcRAP and (*right column*) 10% [2]-GlyRAP sample of microcrystalline α-spectrin SH3. Spectra were recoreded at 20 T (850 MHz), setting the MAS frequency to 40 (50) kHz using the GlcRAP (GlyRAP) sample. On the top (A,B) the full aliphatic spectrum is shown, whereas in the second (C,D), third (E,F) and last row (G,H), the ^{1}Hα,^{13}Cα backbone, side chain and methyl spectral region is represented, respectively. For the 10% [2]-GlyRAP sample, a significant gain in resolution is observed. ^{1}Hα,^{13}Cα correlations for Arg, Gln, Glu and Leu are absent. Intensities for Pro are strongly reduced. In the highlighted side chain region, Glu-Cγ and Lys-Cβ resonances were severely reduced using the [2]-GlyRAP sample. In the methyl region, as expected from the metabolism (Figure S1), only Thr-Cγ2 and Ile-Cδ1 resonances were detectable, while other methyl resonances were efficiently suppressed.

DOI: 10.1021/ja509367q
J. Am. Chem. Soc. 2015, 137, 1094−1100

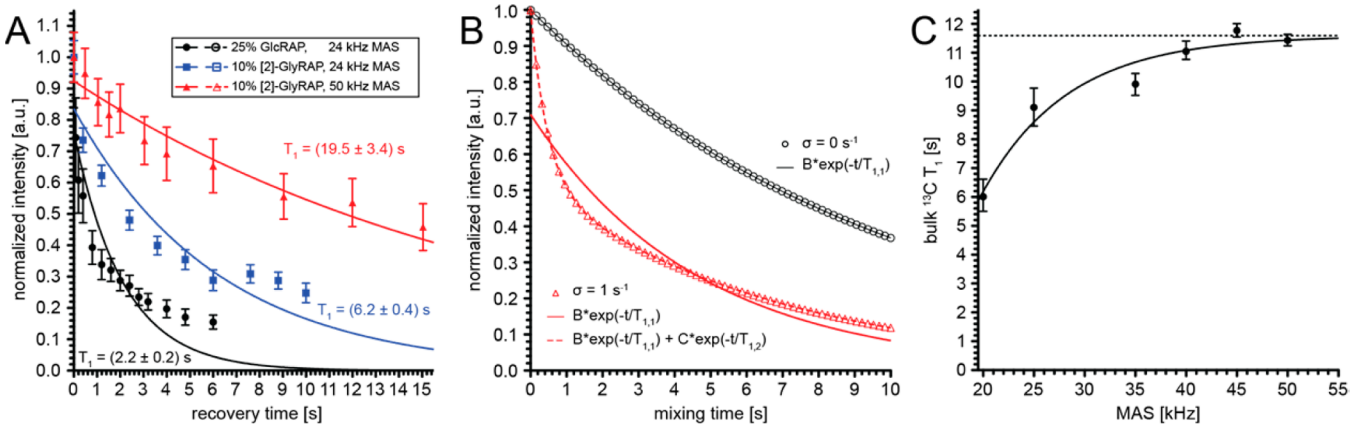

Figure 2. (A) $^{13}C\alpha$ backbone T_1 relaxation curves for Trp41 in a microcrystalline sample of α-spectrin SH3, using a 25% GlcRAP and a 10% [2]-GlyRAP labeling scheme. Spectra were recorded at MAS frequencies of 24 kHz (25% GlcRAP, 10% [2]-GlyRAP at 16.4 T) and 50 kHz (10% [2]-GlyRAP at 20.0 T). Significantly longer T_1 times are obtained for higher MAS frequencies, as well as with increasing dilution of the proton and carbon spin systems. (B) Influence of $^{13}C,^{13}C$ spin diffusion on ^{13}C T_1 relaxation decay curves. Curves are calculated using eq 2. In the absence of spin diffusion (σ = 0.0 s^{-1}, black circles) a monoexponential decay is obtained. Spin diffusion rates $\sigma > 0$ s^{-1} yield a biexponential decay (red triangles). The curves were calculated assuming A_0 = 1.0, B_0 = 0.0, ρ_A = 0.1 s^{-1} and ρ_B = 0.2 s^{-1}, respectively. (C) Bulk experimental $^{13}C\alpha$ T_1 relaxation time as a function of the MAS frequency at an external magnetic field of 11.7 T (500 MHz), using the 10% [2]-GlyRAP α-spectrin SH3 sample. The T_1 relaxation time increases with the MAS frequency, and reaches a plateau at a MAS frequency of 45 kHz. In the experiments, we had to restrict the MAS frequencies to values below 50 kHz as the spinning induced sample heating induced degradation of the sample.

averaged T_1 times.[20−22] Explicit calculations taking MAS into account yield only small deviations from the initial slope approximation.[72,21] For ^{15}N backbone amides which have order parameters $S^2 > 0.7$, the diffusion-in-a-cone approach, employing the "explicit average sum" treatment,[21] yields very similar results as a model-free treatment.[73,52,23] On the other hand, $^{13}C,^{13}C$ spin diffusion can potentially yield an averaging of T_1 times and induces a reduction of the measured rate in case relaxation sinks, such as methyl groups are coupled to the measured nucleus.[13,10]

Figure 2A shows the normalized magnetization decay of the Trp41 $^{13}C\alpha$ backbone resonance as a function of the recovery time for the 25% GlcRAP and the 10% [2]-GlyRAP sample. For the 25% GlcRAP (measured at a MAS frequency of 24 kHz), almost all $^{13}C\alpha-T_1$ curves significantly deviate from a monoexponential relaxation behavior. In general, T_1 relaxation times are very short with an average value of (2.3 ± 0.9) s. A biexponential function yields an adequate fit for all decay curves ($R^2 \geq 0.96$). Figure 2B illustrates the theoretical relaxation behavior of two coupled spins that relax with different autorelaxation rates. For the calculation eq 2 has been employed, assuming an initial magnetization A_0 = 1.0 and B_0 = 0.0 (i.e., spin A is polarized, spin B relaxed back to its equilibrium state). In the example, the autorelaxation rates are set to ρ_A = 0.1 s^{-1} and ρ_B = 0.2 s^{-1}. For σ = 0 s^{-1}, a monoexponential decay is obtained, $[A](t) = e^{-0.1t}$ (Figure 2B, black circles). For σ = 1 s^{-1}, a biexponential decay is obtained, $[A](t) = 0.48e^{-2.15t} + 0.52e^{-0.15t}$ (Figure 2B, red triangles). In that case, a monoexponential fit yields only a poor convergence (solid red line). In order to verify whether the experimental MAS frequency and the employed $^{1}H/^{13}C$ spin dilution is sufficient, we recorded bulk ^{13}C T_1 relaxation times as a function of the MAS frequency (Figure 2C). The bulk ^{13}C T_1 time increases with increasing spinning frequencies and reaches a plateau around 45 kHz. This result is consistent with cross peak intensities in 2D $^{13}C,^{13}C$ PDSD[74] experiments that we recorded as a function of the MAS frequency, as well as the degree of ^{1}H and ^{13}C spin dilution (Figure S3). A 25% GlcRAP sample (τ_{mix} = 2 s, 24 kHz MAS) yields numerous cross-peaks (Figure S3A). The number of cross peaks is already greatly reduced for a 15% GlcRAP sample spun at 50 kHz MAS (τ_{mix} = 3 s, Figure S3C). Almost no cross peaks are observable for a 10% [2]-GlyRAP sample under the same conditions (τ_{mix} = 2 s, 5 s, Figure S3B,D). We note that $^{13}CO,^{13}C\beta$ cross peaks are particularly intense due to the matching of the rotational resonance condition,[75] employing a MAS frequency of 24 kHz at an external magnetic field of 16.4 T (Figure S3A,B).

Therefore, the use of ^{1}H and ^{13}C spin dilute samples, in combination with fast spinning (MAS ≥ 50 kHz), yields monoexponentially decaying ^{13}C T_1 curves (Figure 2A), which exclusively report on local dynamics. Under these conditions, coherent contributions are averaged out.

Backbone $^{13}C\alpha$ T_1 relaxation times for GlcRAP and GlyRAP labeled samples are represented in Figure 3A-D. In general, $^{13}C\alpha$ T_1 increases with MAS, the amount of deuteration and ^{13}C dilution. For the 25% GlcRAP sample (Figure 3D), we obtain very similar $^{13}C\alpha$ T_1 values along the backbone. This indicates that relaxation of nuclear spins is influenced by spin diffusion, which results in a degeneration of the respective rates. This is consistent with the observation of $^{13}C,^{13}C$ PDSD cross peaks (Figure S3A). For the 15% GlcRAP sample (Figure 3C), $^{13}C\alpha$ T_1 relaxation times are already significantly increased. However, also there, a pronounced pattern with fluctuations along the backbone is still not observable. The increased $^{13}C\alpha$ T_1 relaxation times (Figure 3C versus Figure 3D) are predominantly due to the increased MAS rotation frequency. Large site-specific variations become observable in case a 10% [2]-GlyRAP sample is employed in which both the carbon and the proton spins are dilute (Figure 3A and B). Most strinkingly, we find that proton mediated spin diffusion is essentially suppressed by carbon spin dilution (Figure 3B and C). This is due to the fact that HC/CC and CC/CC cross terms are truncated in carbon spin dilute samples (Gromek et al., 2006).[76] We find that the ^{13}C T_1 values in the 10% [2]-GlyRAP sample show a field dependence and increase with higher external magnetic fields (Figure 3A and B). The bulk ^{13}C T_1

DOI: 10.1021/ja509367q
J. Am. Chem. Soc. 2015, 137, 1094−1100

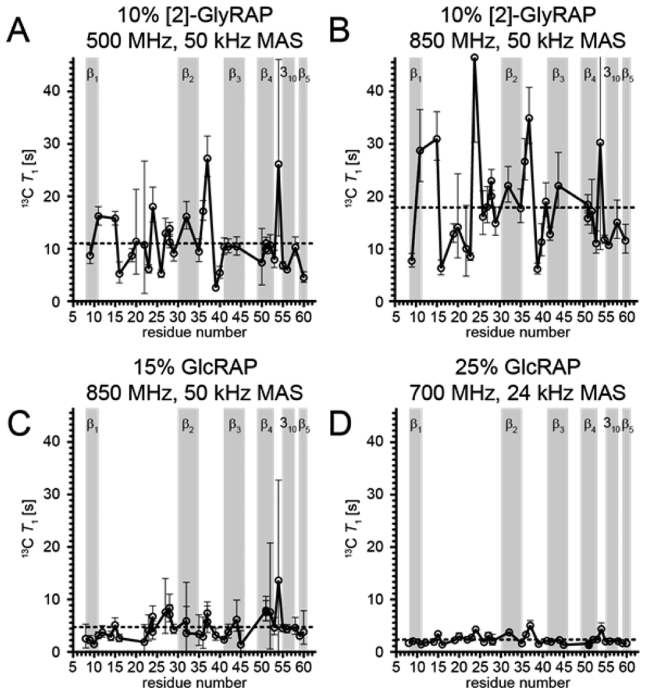

Figure 3. (A–D) Backbone $^{13}C\alpha$ T_1 relaxation times for a 10% [2]-GlyRAP, 15 and 25% GlcRAP microcrystalline sample of α-spectrin SH3 measured at an external magnetic field of 11.7, 16.4, 20.0 T (500, 700, 850 MHz) and a MAS frequency of 24 and 50 kHz, respectively. T_1 relaxation times for the GlcRAP samples are extracted using a monoexponential fitting function. The T_1 errors were estimated using Monte Carlo simulations taking intensity fluctuations due to noise into account ($2\sigma_{noise}$). The dashed horizontal line depicts the average T_1 value for all residues. The secondary structure elements are indicated by gray bars.

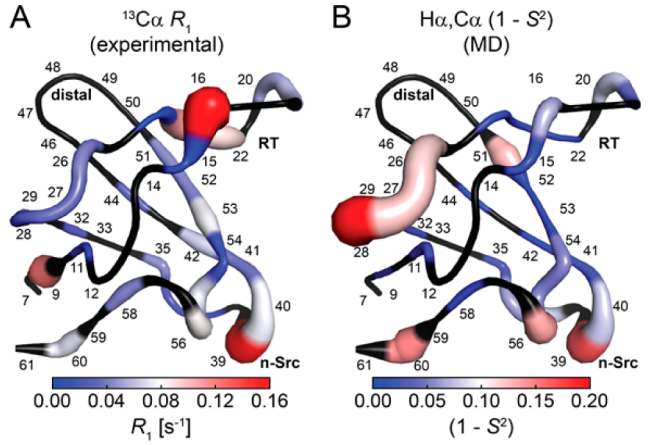

Figure 4. (A) Experimental R_1 rates and (B) MD derived generalized order parameters $(1 - S^2)$ for the Cα backbone atoms of α-spectrin SH3. The experimental R_1 (= $1/T_1$) rates were obtained from the 10% [2]-GlyRAP sample (measured at 850 MHz). The MD trajectory was sampled for 97 ns, employing 8 (crystal) unit cells containing 4 SH3 molecules each. Experimental and MD derived parameters indicate dynamics in similar regions of the structure. The color coding is given at the bottom of the figures. The magnitude of the values is represented by the thickness of the backbone. Residues color coded in black were not employed in the analysis due to spectral overlap or sensitivity issues.

time at 500 and 850 MHz are (11.0 ± 5.6) s and (17.9 ± 9.0) s, respectively. This finding can be attributed to the presence of slow dynamics in the solid-state, and was observed previously for ^{15}N backbone T_1 relaxation times.[41]

Comparison of Experimental $^{13}C\alpha$ T_1 Relaxation Times with MD Simulations. In Figure 4A, the $^{13}C\alpha$ R_1 rates (10% [2]-GlyRAP, 850 MHz) are plotted on the crystal structure of the SH3 domain (PDB ID: 2NUZ).[62] The magnitude of the R_1 rate is represented by the thickness of the backbone. The α-spectrin SH3 domain folds into a barrel like structure, containing five antiparallel β-strands and three loops, namely the RT, the n-Src and the distal loop, respectively.[77] The RT and the n-Src loop are particularly important for binding of proline-rich ligands.[78,79] High $^{13}C\alpha$ R_1 rates, which presumably reflect dynamic residues, cluster in these two loops. Although various SH3 domains adopt a highly similar β-barrel fold, different conformations were found for the RT and n-Src loops.[80−82] As the flanking sequence of a ligand binds to the groove between these two loops, the interaction of the ligand and both loops is fundamental for sequence specificity. We speculate that the required plasticity of both loops is reflected in the measured R_1 rates.

MD simulation is a complementary tool for the determination of protein dynamics.[83−86] To further validate the measured $^{13}C\alpha$ relaxation times, we compared the experimental $^{13}C\alpha$ R_1 rates with order parameters obtained from a MD trajectory. In the calculation, each unit cell contained four SH3 molecules. Employing periodic boundary conditions, the simulation was performed for 8 unit cells. The trajectory was calculated for 97 ns. This trajectory was employed to determine the correlation functions of Hα,Cα backbone dipolar vectors. The correlation function $C(t)$ yields directly information on the generalized order parameter S^2. In Figure 4B, $(1 - S^2)$ is plotted onto the structure. Large $(1 - S^2)$ values and high R_1 rates indicate large amplitude dynamics. We find that $^{13}C\alpha$ R_1 rates and the MD simulation follow the same trend: Especially large motion is observed in the RT and in the n-Src loop. Missing data is due to the labeling scheme, as Arg, Gln, Glu, Leu, Pro $^{13}C\alpha$ incorporation yields are low. Furthermore, resonance assignments were obtained using cross-polarization (CP) based experiments. Information on the dynamics of especially the distal loop is therefore lacking (Figure S8).[26] In the future, scalar-based assignment experiments and access to [1,3]-GlyRAP samples will allow to yield a more complete $^{13}C\alpha$ R_1 data set. Similarly, HNCO type experiments will allow to determine carbonyl relaxation rates in carbon spin dilute samples.

■ DISCUSSION

We suggest here to employ fast MAS in combination with sparse labeling (^1H and ^{13}C) to access ^{13}C R_1 relaxation rates. Both preconditions have to be met for the following reasons:

(i) Fast MAS (>40 kHz) yields an increase in resolution due to averaging of coherent contributions to the line width.[87,27]

(ii) Scalar coupling based ^{13}C T_1 experiments (refocused INEPT schemes, Figure S5B) yield an improvement in sensitivity at high MAS frequencies in comparison to dipolar based experiments.[27]

(iii) The rate of spin diffusion is dependent on the inverse distance of the dipolar coupled spins ($r_{i,j}^{-6}$), the isotropic chemical shift difference of spin i and j, and scales inversely with the magic-angle rotation frequency.[11,12] Accordingly, fast spinning decreases spin diffusion and facilitates the measurement of atom-specific relaxation rates R_1 that report on local

DOI: 10.1021/ja509367q
J. Am. Chem. Soc. 2015, 137, 1094−1100

motion. The effects of spin diffusion can be appreciated from Figure 2B.

(iv) Paramagnetic relaxation enhancement (PRE) is a further potential mechanism that can distort the experimentally observed T_1 relaxation times.[88−92] PRE is induced by paramagnetic impurities such as dissolved oxygen in the crystal lattice. As a result, the theoretical and experimental ^{19}F T_1 times for CaF_2 deviate by a factor of about 10^6.[89] In this present study, α-spectrin SH3 was crystallized from solvent. Potential paramagnetic impurities are primarily bound to water molecules and tumble rapidly which in turn reduces the PRE effect in the microcrystals. We assume therefore that the PRE effect in microcrystalline α-spectrin SH3 has a similar order of magnitude as α-spectrin SH3 in solution. This assumption is supported by the fact that experimental ^{13}C methyl T_1, as well as ^{15}N T_1 times in the solid and the solution are highly correlated.[39,22] We observe furthermore a good agreement with the MD simulation, which suggests that the influence of paramagnetic impurities can be largely neglected.

(v) We observe a biexponential decay of the experimental $^{13}C\alpha$ T_1 relaxation times (Figure 2A/B) in case a non ^{13}C spin dilute sample is employed (GlcRAP). We expect that coherent effects are even more detrimental in case protonated samples are employed. These results make it questionable whether protonated and uniformly carbon labeled protein samples are suitable to quantify protein dynamics based on $^{13}C\alpha$ relaxation experiments even at 60 kHz MAS.[13]

CONCLUSIONS

We could show that the [2]-GlyRAP labeling scheme presented here yields sparsely ^{13}C labeled proteins in a deuterated matrix. [2]-GlyRAP samples show enhanced resolution due to a lower number of labels and missing $^1J(^{13}C,^{13}C)$ scalar couplings. The labeling scheme enables spectral editing, as only a defined set of peaks is obtained in the spectra (e.g., the $^1H\alpha,^{13}C\alpha$ resonances of Arg, Gln, Glu, Leu, Pro, as well as methyl resonances of Ala, Ile-Cγ2, Leu, Met and Val and further side chain resonances are reduced). The labeling scheme is furthermore ideally suited for the quantification of dynamics of side chain and backbone carbons in a protein in the solid-state. Application of ^1H detection allows to improve the experimental sensitivity and the accuracy of the determined relaxation parameters. The combination of sparse labeling, deuteration and fast magic angle spinning reduces $^{13}C,^{13}C$ spin diffusion to an undetectable level, in particular when aliphatic carbons are considered. Qualitatively, we find good agreement between the $^{13}C\alpha$ R_1 relaxation rates and the generalized order parameters $(1 - S^2)$ from MD simulations indicating a high degree of flexibility in two loops of the α-spectrin SH3 domain. We conclude that ^1H and ^{13}C spin dilute samples, such as the 10% [2]-GlyRAP sample, have to be employed for a proper quantification of $^{13}C\alpha$ dynamics, as otherwise spin diffusion, especially involving methyl groups, can effectively shorten the apparent T_1 relaxation times. In the future, we will explore [1,3]-GlyRAP labeled samples, which will give access to a complementary set of nuclei and thus allow to complete the relaxation data set.

ASSOCIATED CONTENT

Supporting Information

Additional figures showing side chain labeling patterns, full spectrum of [2]-GlyRAP and GlcRAP labeled SH3, 2D-$^{13}C,^{13}C$ PDSD spectra, simulations of the influence of CSA on ^{13}C and ^{15}N T_1, as well as of ^{13}C T_1 as a function of the order parameters S_S^2 and τ_S in solution and in the solid-state, NMR pulse schemes, ^{13}C T_1 relaxation decay curves, and MD derived order parameters. This material is available free of charge via the Internet at http://pubs.acs.org.

AUTHOR INFORMATION

Corresponding Author

reif@tum.de

Notes

The authors declare no competing financial interest.

ACKNOWLEDGMENTS

This work was supported by the Helmholtz-Gemeinschaft, the Deutsche Forschungsgemeinschaft (Grants Re1435, SFB1035) and the Bio-NMR project (European Commission's Framework Program 7, project number: 261863/BIO-NMR-00010, BIO-NMR-00070). We are grateful to the Center for Integrated Protein Science Munich (CIPS-M) for financial support and to B. H. Meier (ETH Zürich) for providing measurement time, as well as to Bruker BioSpin, especially to S. Wegner. We acknowledge K. Szekely (ETH Zürich) for technical support.

REFERENCES

(1) Mainz, A.; Jehle, S.; van Rossum, B. J.; Oschkinat, H.; Reif, B. *J. Am. Chem. Soc.* **2009**, *131*, 15968.
(2) Bertini, I.; Luchinat, C.; Parigi, G.; Ravera, E.; Reif, B.; Turano, P. *Proc. Natl. Acad. Sci. U. S. A.* **2011**, *108*, 10396.
(3) Knight, M. J.; Webber, A. L.; Pell, A. J.; Guerry, P.; Barbet-Massin, E.; Bertini, I.; Felli, I. C.; Gonnelli, L.; Pierattelli, R.; Emsley, L.; Lesage, A.; Herrmann, T.; Pintacuda, G. *Angew. Chem., Int. Ed. Engl.* **2011**, *50*, 11697.
(4) Loquet, A.; Sgourakis, N. G.; Gupta, R.; Giller, K.; Riedel, D.; Goosmann, C.; Griesinger, C.; Kolbe, M.; Baker, D.; Becker, S.; Lange, A. *Nature* **2012**, *486*, 276.
(5) Park, S. H.; Das, B. B.; Casagrande, F.; Tian, Y.; Nothnagel, H. J.; Chu, M. N.; Kiefer, H.; Maier, K.; De Angelis, A. A.; Marassi, F. M.; Opella, S. J. *Nature* **2012**, *491*, 779.
(6) Mainz, A.; Religa, T. L.; Sprangers, R.; Linser, R.; Kay, L. E.; Reif, B. *Angew. Chem., Int. Ed. Engl.* **2013**, *52*, 8746.
(7) Levy, R. M.; Karplus, M.; Mccammon, J. A. *J. Am. Chem. Soc.* **1981**, *103*, 994.
(8) Karplus, M.; Petsko, G. A. *Nature* **1990**, *347*, 631.
(9) Henzler-Wildman, K. A.; Lei, M.; Thai, V.; Kerns, S. J.; Karplus, M.; Kern, D. *Nature* **2007**, *450*, 913.
(10) Fry, E. A.; Sengupta, S.; Phan, V. C.; Kuang, S.; Zilm, K. W. *J. Am. Chem. Soc.* **2011**, *133*, 1156.
(11) Kubo, A.; Mcdowell, C. A. *J. Chem. Soc., Faraday Trans. I* **1988**, *84*, 3713.
(12) Lange, A.; Seidel, K.; Verdier, L.; Luca, S.; Baldus, M. *J. Am. Chem. Soc.* **2003**, *125*, 12640.
(13) Lewandowski, J. R.; Sein, J.; Sass, H. J.; Grzesiek, S.; Blackledge, M.; Emsley, L. *J. Am. Chem. Soc.* **2010**, *132*, 8252.
(14) Krushelnitsky, A.; Brauniger, T.; Reichert, D. *J. Magn. Reson.* **2006**, *182*, 339.
(15) Giraud, N.; Blackledge, M.; Bockmann, A.; Emsley, L. *J. Magn. Reson.* **2007**, *184*, 51.
(16) Kuhlmann, K. F.; Grant, D. M.; Harris, R. K. *J. Chem. Phys.* **1970**, *52*, 3439.
(17) Allerhand, A.; Doddrell, D.; Glushko, U.; Cochran, D. W.; Wenkert, E.; Lawson, P. J.; Gurd, F. R. N. *J. Am. Chem. Soc.* **1971**, *93*, 544.
(18) Kay, L. E.; Torchia, D. A.; Bax, A. *Biochemistry* **1989**, *28*, 8972.
(19) Mittermaier, A.; Kay, L. E. *Science* **2006**, *312*, 224.
(20) Torchia, D. A.; Szabo, A. *J. Magn. Reson.* **1982**, *49*, 107.

DOI: 10.1021/ja509367q
J. Am. Chem. Soc. 2015, 137, 1094−1100

(21) Giraud, N.; Blackledge, M.; Goldman, M.; Bockmann, A.; Lesage, A.; Penin, F.; Emsley, L. *J. Am. Chem. Soc.* **2005**, *127*, 18190.
(22) Agarwal, V.; Xue, Y.; Reif, B.; Skrynnikov, N. R. *J. Am. Chem. Soc.* **2008**, *130*, 16611.
(23) Schanda, P.; Meier, B. H.; Ernst, M. *J. Am. Chem. Soc.* **2010**, *132*, 15957.
(24) LeMaster, D. M.; Kushlan, D. M. *J. Am. Chem. Soc.* **1996**, *118*, 9255.
(25) Asami, S.; Schmieder, P.; Reif, B. *J. Am. Chem. Soc.* **2010**, *132*, 15133.
(26) Asami, S.; Reif, B. *J. Biomol. NMR* **2012**, *52*, 31.
(27) Asami, S.; Szekely, K.; Schanda, P.; Meier, B. H.; Reif, B. *J. Biomol. NMR* **2012**, *54*, 155.
(28) Asami, S.; Reif, B. *Acc. Chem. Res.* **2013**, *46*, 2089.
(29) Chevelkov, V.; Rehbein, K.; Diehl, A.; Reif, B. *Angew. Chem., Int. Ed.* **2006**, *45*, 3878.
(30) Bockmann, A.; Gardiennet, C.; Verel, R.; Hunkeler, A.; Loquet, A.; Pintacuda, G.; Emsley, L.; Meier, B. H.; Lesage, A. *J. Biomol. NMR* **2009**, *45*, 319.
(31) Huber, M.; With, O.; Schanda, P.; Verel, R.; Ernst, M.; Meier, B. H. *J. Magn. Reson.* **2012**, *214*, 76.
(32) Shaka, A. J.; Keeler, J.; Frenkiel, T.; Freeman, R. *J. Magn. Reson.* **1983**, *52*, 335.
(33) Paulson, E. K.; Morcombe, C. R.; Gaponenko, V.; Dancheck, B.; Byrd, R. A.; Zilm, K. W. *J. Am. Chem. Soc.* **2003**, *125*, 15831.
(34) Zhou, D. H.; Rienstra, C. M. *J. Magn. Reson.* **2008**, *192*, 167.
(35) Kay, L. E.; Nicholson, L. K.; Delaglio, F.; Bax, A.; Torchia, D. A. *J. Magn. Reson.* **1992**, *97*, 359.
(36) Palmer, A. G.; Skelton, N. J.; Chazin, W. J.; Wright, P. E.; Rance, M. *Mol. Phys.* **1992**, *75*, 699.
(37) Yamazaki, T.; Muhandiram, R.; Kay, L. E. *J. Am. Chem. Soc.* **1994**, *116*, 8266.
(38) Shajani, Z.; Varani, G. *J. Mol. Biol.* **2005**, *349*, 699.
(39) Chevelkov, V.; Zhuravleva, A. V.; Xue, Y.; Reif, B.; Skrynnikov, N. R. *J. Am. Chem. Soc.* **2007**, *129*, 12594.
(40) Sein, J.; Giraud, N.; Blackledge, M.; Emsley, L. *J. Magn. Reson.* **2007**, *186*, 26.
(41) Chevelkov, V.; Diehl, A.; Reif, B. *J. Chem. Phys.* **2008**, *128*, 052316.
(42) Sklenar, V.; Torchia, D.; Bax, A. *J. Magn. Reson.* **1987**, *73*, 375.
(43) Abragam, A. *The Principles of Nuclear Magnetism*; Clarendon Press: Oxford, U.K., 1961.
(44) Alkaraghouli, A. R.; Koetzle, T. F. *Acta Crystallogr., Sect. B: Struct. Sci.* **1975**, *31*, 2461.
(45) Yao, X. L.; Schmidt-Rohr, K.; Hong, M. *J. Magn. Reson.* **2001**, *149*, 139.
(46) Yao, L. S.; Vogeli, B.; Ying, J. F.; Bax, A. *J. Am. Chem. Soc.* **2008**, *130*, 16518.
(47) Brown, M. F. *J. Chem. Phys.* **1982**, *77*, 1576.
(48) Lipari, G.; Szabo, A. *J. Am. Chem. Soc.* **1982**, *104*, 4559.
(49) Lipari, G.; Szabo, A. *J. Am. Chem. Soc.* **1982**, *104*, 4546.
(50) Brown, M. F. *J. Chem. Phys.* **1984**, *80*, 2808.
(51) Clore, G. M.; Szabo, A.; Bax, A.; Kay, L. E.; Driscoll, P. C.; Gronenborn, A. M. *J. Am. Chem. Soc.* **1990**, *112*, 4989.
(52) Chevelkov, V.; Fink, U.; Reif, B. *J. Biomol. NMR* **2009**, *45*, 197.
(53) Wu, C. H.; Ramamoorthy, A.; Gierasch, L. M.; Opella, S. J. *J. Am. Chem. Soc.* **1995**, *117*, 6148.
(54) Chekmenev, E. Y.; Zhang, Q. W.; Waddell, K. W.; Mashuta, M. S.; Wittebort, R. J. *J. Am. Chem. Soc.* **2004**, *126*, 379.
(55) Tjandra, N.; Bax, A. *J. Am. Chem. Soc.* **1997**, *119*, 8076.
(56) Tjandra, N.; Bax, A. *J. Am. Chem. Soc.* **1997**, *119*, 9576.
(57) Fushman, D.; Tjandra, N.; Cowburn, D. *J. Am. Chem. Soc.* **1998**, *120*, 10947.
(58) Wylie, B. J.; Schwieters, C. D.; Oldfield, E.; Rienstra, C. M. *J. Am. Chem. Soc.* **2009**, *131*, 985.
(59) Wylie, B. J.; Sperling, L. J.; Nieuwkoop, A. J.; Franks, W. T.; Oldfield, E.; Rienstra, C. M. *Proc. Natl. Acad. Sci. U. S. A.* **2011**, *108*, 16974.
(60) Macura, S.; Ernst, R. R. *Mol. Phys.* **1980**, *41*, 95.
(61) Engelke, J.; Ruterjans, H. *J. Biomol. NMR* **1995**, *5*, 173.
(62) Chevelkov, V.; Faelber, K.; Schrey, A.; Rehbein, K.; Diehl, A.; Reif, B. *J. Am. Chem. Soc.* **2007**, *129*, 10195.
(63) Hess, B.; Kutzner, C.; van der Spoel, D.; Lindahl, E. *J. Chem. Theory Comput.* **2008**, *4*, 435.
(64) Hess, B. *J. Chem. Theory Comput.* **2007**, *4*, 116.
(65) Miyamoto, S.; Kollman, P. A. *J. Comput. Chem.* **1992**, *13*, 952.
(66) Essmann, U.; Perera, L.; Berkowitz, M. L.; Darden, T.; Lee, H.; Pedersen, L. G. *J. Chem. Phys.* **1995**, *103*, 8577.
(67) Bussi, G.; Donadio, D.; Parrinello, M. *J. Chem. Phys.* **2007**, *126*, 014101.
(68) Smith, P. E.; van Schaik, R. C.; Szyperski, T.; Wuthrich, K.; van Gunsteren, W. F. *J. Mol. Biol.* **1995**, *246*, 356.
(69) Cerutti, D. S.; Freddolino, P. L.; Duke, R. E., Jr.; Case, D. A. *J. Phys. Chem. B* **2010**, *114*, 12811.
(70) Mollica, L.; Baias, M.; Lewandowski, J. R.; Wylie, B. J.; Sperling, L. J.; Rienstra, C. M.; Emsley, L.; Blackledge, M. *J. Phys. Chem. Lett.* **2012**, *3*, 3657.
(71) Xue, Y.; Skrynnikov, N. R. *Protein Sci.* **2014**, *23*, 488.
(72) Lipari, G.; Szabo, A. *J. Chem. Phys.* **1981**, *75*, 2971.
(73) Skrynnikov, N. R. *Magn. Reson. Chem.* **2007**, *45*, S161.
(74) Szeverenyi, N. M.; Sullivan, M. J.; Maciel, G. E. *J. Magn. Reson.* **1982**, *47*, 462.
(75) Raleigh, D. P.; Levitt, M. H.; Griffin, R. G. *Chem. Phys. Lett.* **1988**, *146*, 71.
(76) Grommek, A.; Meier, B. H.; Ernst, M. *Chem. Phys. Lett.* **2006**, *427*, 404.
(77) Camara-Artigas, A.; Andujar-Sanchez, M.; Ortiz-Salmeron, E.; Cuadri, C.; Cobos, E. S.; Martin-Garcia, J. M. *Acta Crystallogr., Sect. F: Struct. Biol. Cryst. Commun.* **2010**, *66*, 1023.
(78) Cicchetti, P.; Mayer, B. J.; Thiel, G.; Baltimore, D. *Science* **1992**, *257*, 803.
(79) Ren, R. B.; Mayer, B. J.; Cicchetti, P.; Baltimore, D. *Science* **1993**, *259*, 1157.
(80) Feng, S. B.; Kasahara, C.; Rickles, R. J.; Schreiber, S. L. *Proc. Natl. Acad. Sci. U. S. A.* **1995**, *92*, 12408.
(81) Morken, J. P.; Kapoor, T. M.; Feng, S. B.; Shirai, F.; Schreiber, S. L. *J. Am. Chem. Soc.* **1998**, *120*, 30.
(82) Kay, B. K.; Williamson, M. P.; Sudol, P. *FASEB J.* **2000**, *14*, 231.
(83) Prompers, J. J.; Bruschweiler, R. *J. Am. Chem. Soc.* **2002**, *124*, 4522.
(84) Chen, J.; Brooks, C. L., 3rd; Wright, P. E. *J. Biomol. NMR* **2004**, *29*, 243.
(85) Nederveen, A. J.; Bonvin, A. M. J. J. *J. Chem. Theory Comput.* **2005**, *1*, 363.
(86) Showalter, S. A.; Brüschweiler, R. *J. Chem. Theory Comput.* **2007**, *3*, 961.
(87) Lewandowski, J. R.; Sass, H. J.; Grzesiek, S.; Blackledge, M.; Emsley, L. *J. Am. Chem. Soc.* **2011**, *133*, 16762.
(88) Rollin, B. V.; Hatton, J. *Phys. Rev.* **1948**, *74*, 346.
(89) Bloembergen, N. *Physica* **1949**, *15*, 386.
(90) Clore, G. M.; Iwahara, J. *Chem. Rev.* **2009**, *109*, 4108.
(91) Wickramasinghe, N. P.; Parthasarathy, S.; Jones, C. R.; Bhardwaj, C.; Long, F.; Kotecha, M.; Mehboob, S.; Fung, L. W.; Past, J.; Samoson, A.; Ishii, Y. *Nat. Methods* **2009**, *6*, 215.
(92) Panich, A. M.; Furman, G. B. *Diamond Relat. Mater.* **2012**, *23*, 157.

DOI: 10.1021/ja509367q
J. Am. Chem. Soc. 2015, 137, 1094−1100